



Efficiently photoelectrocatalyze CO_2 to methanol using Ru(II)-pyridyl complex covalently bonded on TiO_2 nanotube arrays

Jibo Liu, Huijie Shi, Qi Shen, Chenyan Guo, Guohua Zhao*

School of Chemical Science and Engineering, Shanghai Key Lab of Chemical Assessment and Sustainability, Tongji University, 1239 Siping Road, Shanghai 200092, China

ARTICLE INFO

Article history:

Received 20 December 2016

Received in revised form 16 March 2017

Accepted 24 March 2017

Available online 27 March 2017

Keywords:

CO_2 reduction

Methanol

Metal-organic complex

Covalent linking

Pyridiniumformate

ABSTRACT

Aiming at improving the efficiency of photoelectrocatalytic (PEC) CO_2 conversion to methanol, a heterogeneous photoelectrocatalyst was prepared by covalently binding a Ru(II) metal-organic complex (Ru-Py) containing exposed pyridyl on the periodic TiO_2 nanotube arrays (TNTAs). PEC characterization indicated that the Ru-Py/TNTAs photocathode exhibited excellent PEC CO_2 reduction activity in aqueous solution. The initial CO_2 reduction potential on Ru-Py/TNTAs photocathode reached -0.4 V (vs. NHE) under simulated solar irradiation. The cathodic photocurrent response of Ru-Py/TNTAs in CO_2 -saturated aqueous solution was about 1.79 mA cm^{-2} , which was 2.4 times that of TNTAs. It may be caused by the enhanced light absorption in the visible region originated from Ru-Py. Meanwhile, Ru-Py played an important role in accelerating the separation of photoinduced electron-hole pairs evidenced by the photoluminescence spectra. PEC CO_2 reduction test showed that $84.8\text{ }\mu\text{mol}$ methanol was produced with 63.9% faraday efficiency, 62.6 turnover number (TON) and 45% selectivity at -0.9 V under 8 h irradiation. Furthermore, the non-covalent bonded system only produced $41.3\text{ }\mu\text{mol}$ methanol indicating that the carboxylic covalent linking displayed excellent electron transfer efficiency and methanolization performance. The mechanism investigation revealed that the exposed pyridyl provided the active sites in forming pyridiniumformate intermediates confirmed by the differential UV-vis absorption (ΔA) spectrum, which was of great significance in the efficient CO_2 methanolization. The probable reaction pathway for catalytic CO_2 reduction to methanol was also proposed combining the possible intermediates detected by gas chromatography mass spectrometry (GCMS).

© 2017 Elsevier B.V. All rights reserved.

1. Introduction

The atmospheric carbon dioxide (CO_2) levels has raised up to 400 mg l^{-1} due to the large scale consumption of fossil fuels (such as coal, natural gas and petroleum) for the energy production over the last century [1–3]. The global warming and energy shortage are the two global urgent problems caused by higher CO_2 emission and energy excessive consumption [4,5]. The photochemical (PC), electrochemical (EC) and photoelectrochemical (PEC) conversion of CO_2 to the liquid fuels for instance methanol, formic acid et al. based on solar irradiation could help at some extent to decrease the CO_2 content in the environment and avail the increasing demand of energy [6,7]. Especially, CO_2 hydrogenation to methanol was a remarkable thing because methanol is an important feedstock for

the organic chemical industry and a potential alternative to fossil fuels [8,9].

However, efficient conversion of CO_2 into methanol was still a challenge because of the stable thermodynamic property and intricate reduction product of CO_2 [10]. For CO_2 high efficiency conversion, the scientists have made significant contributions, particularly in the fundamental understanding of using transition-metal complexes, metal organic framework (MOFs), imidazolium ionic liquids and heterocyclic compound as catalysts [11–17]. Photoelectrocatalysis by organic molecules or metal-organic complexes is a viable measure for excellent tunability and selectivity to CO_2 reduction caused by the regulated reaction sites [18,19]. Literature research indicated that pyridine (Py) is one of the typical heterocyclic organic molecule to catalyze CO_2 into methanol [20–24]. Activated CO_2 inserts into N–H bond of the protonated Py (PyH^+) to form a pyridiniumformate intermediate which can be further reduced to give the 6e migration product [14]. But the high methanolization efficiency was only displayed on some noble metal electrodes (Pt, Pd) and limited kinds of semiconductor pho-

* Corresponding author.

E-mail address: g.zhao@tongji.edu.cn (G. Zhao).

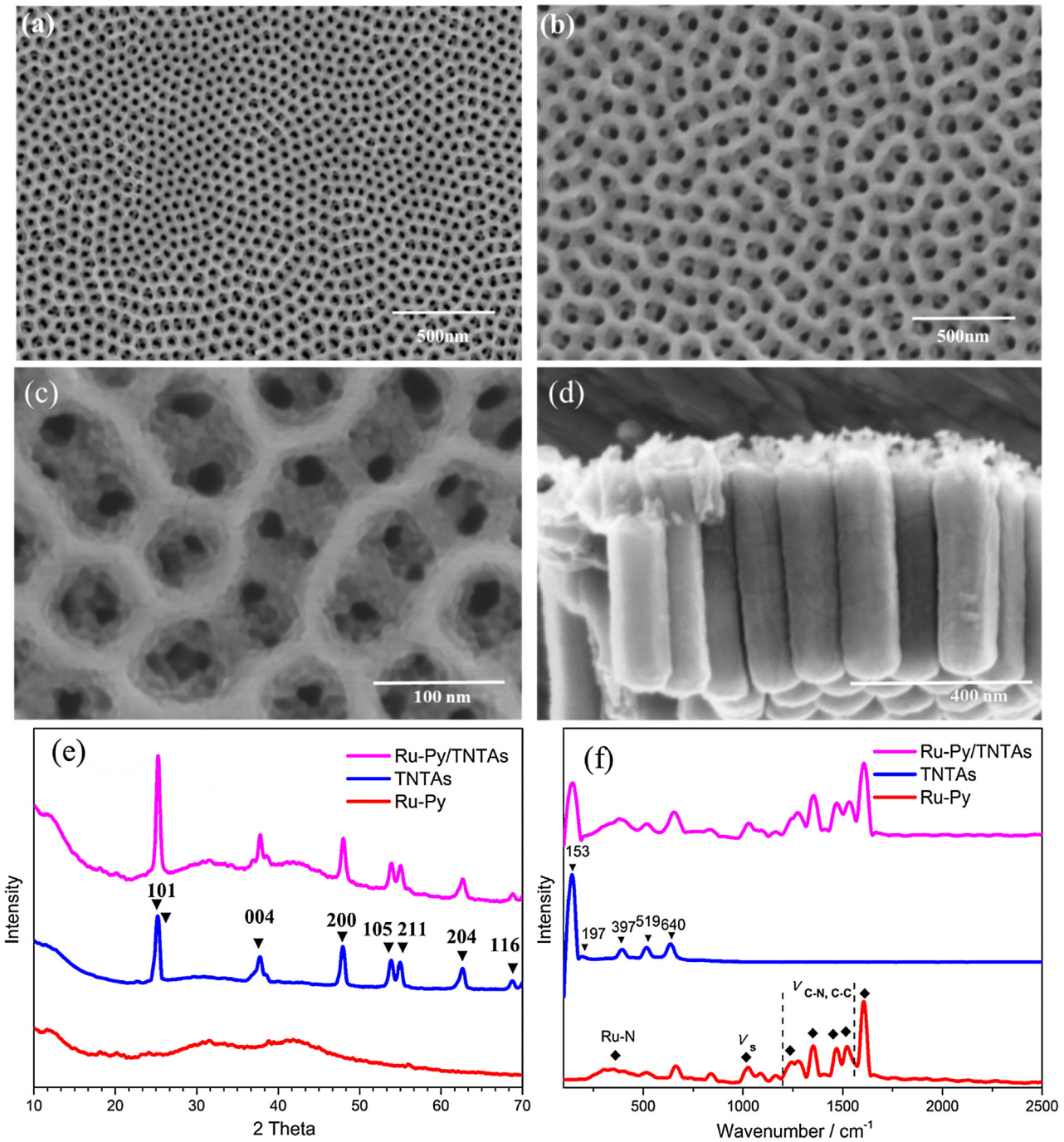


Fig. 1. (a) Scanning electron micrographs (SEM) of TNTAs obtained from a three-step electrochemical anodization; (b) SEM image of Ru-Py/TNTAs; (c) a high magnification of Ru-Py/TNTAs; (d) Cross-sectional SEM image of TNTAs; (e) XRD patterns of TNTAs, Ru-Py and Ru-Py/TNTAs; (d) Raman spectra of TNTAs, Ru-Py and Ru-Py/TNTAs.

toelectroelectrodes such as *n*-GaP, *p*-GaAs and *p*-InP in aqueous solution containing 5–10 mM pyridine, no matter under electrocatalytic condition or photocatalytic condition [14,24–26]. In contrast, unimolecular photoelectrocatalyst incorporating both the metal-organic complex photosensitizer and the exposed pyridyl subunit showed higher CO₂ methanolization efficiency and selectivity for methanol than photosensitizer separated with pyridine system [27]. However, the unimolecular photocatalytic system took place in homogeneous organic solution which showed disadvantageous characters such as large catalyst demand and difficult to reclaim [1]. Furthermore, the homogeneous reaction was not good for utilization ratio of optical energy due to the dark col-

ors of most metal-organic complexes showing which limited the light into the inside molecules in the solution. More importantly, in homogeneous aqueous solution, the photocatalytic activity of the metal-organic complex also decreased due to the photo-corrosion and dimerization [28]. Heterogeneous catalysis provided an important way to overcome the shortage caused by homogeneous reaction in which the catalytic activity of the metal-organic complex was well maintained. Covalent linking the metal-organic complex on a semiconductor electrode by the organic functional group anchoring was a classical method which could not only translate the homogeneous catalyst to heterogeneous catalyst but also

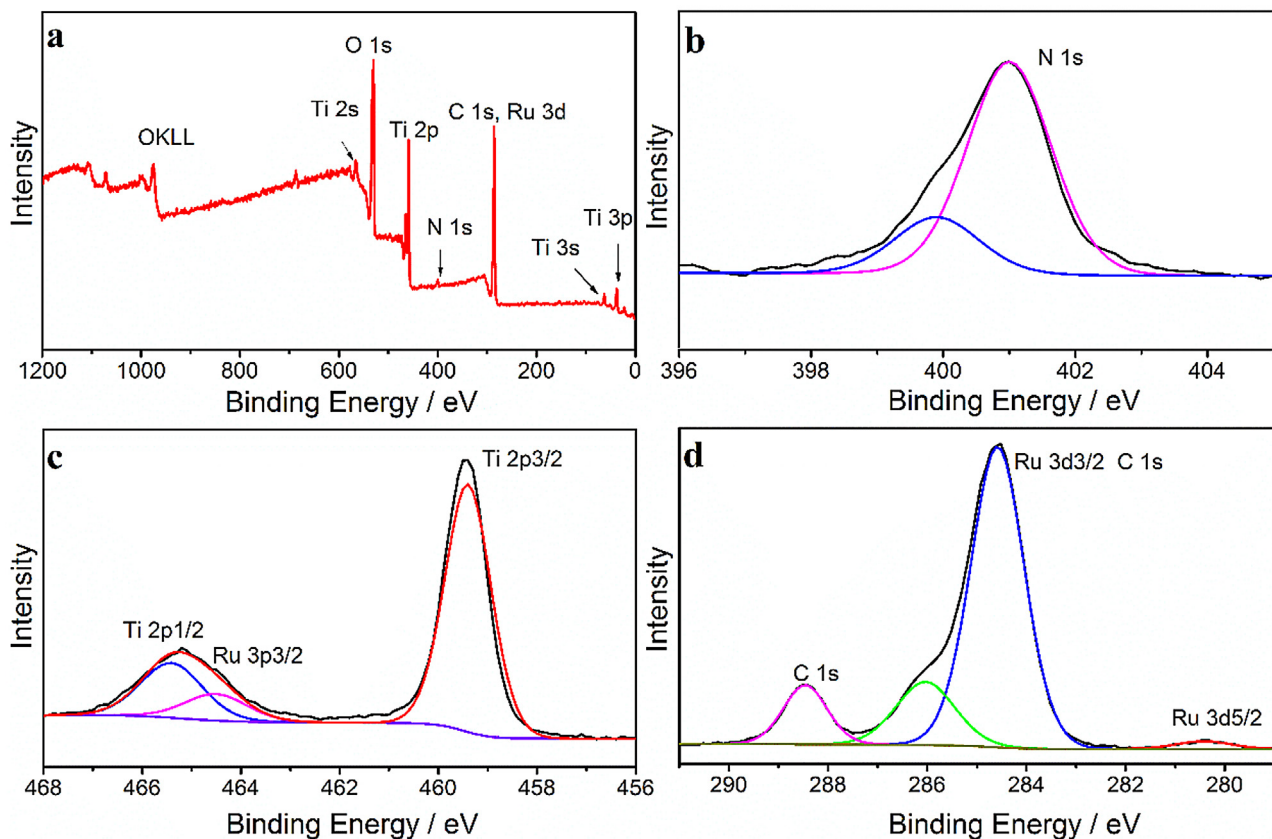


Fig. 2. (a) XPS survey scan of as-prepared Ru-Py/TNTAs electrodes; High-resolution XPS core level spectra (b) N 1s, (c) Ti 2p, Ru 3p and (d) C 1s, Ru 3d of Ru-Py/TNTAs.

promote the efficiency of electron transfer from one side to the other [29,30].

Many semiconductors, especially TiO_2 had attracted a wide spread attention in PEC CO_2 reduction and water oxidation due to the excellent properties such as low-cost, non-toxic, chemical stable, superior light harvest and so on [31–34]. However, the photoinduced electron-hole recombination of TiO_2 decreased the application in CO_2 reduction [35]. It was reported that the surface modification could not only decrease the electron-hole recombination of TiO_2 efficiently but also restrain the photocorrosion of metal-organic complex [18,28].

Herein, a Ru (II) metal-organic complex (Ru-Py, all the structure involved in this paper was shown in Supporting information) photoelectrocatalyst containing exposed pyridyl was prepared and covalently linked on the surface of TNTAs photocathode. Due to the synergistic effect of Ru-Py and TNTAs on light harvest, the absorption band edge extended to nearly 900 nm which resulted in obviously increased photocurrent in CO_2 saturated aqueous solution compared with that of bare TNTAs. The Ru(II) complex containing exposed pyridyl give 6.0 μmol methanol in organic homogeneous solution whereas the Ru-Py/FTO electrode (FTO: fluorine-doped tin oxide coated glass) produce 27.6 μmol methanol with 30.1% faraday efficiency in aqueous solution [27]. On TNTAs covalently linked with Ru-Py, the methanol production increased to 84.8 μmol with 63.9% faraday efficiency. For elucidating the mechanism of CO_2 reduction, the band alignment and the photoinduced electron migration were discussed by combination of the photoluminescence spectra and UV-vis DRS etc. The photoinduced electrons on the conduction band of TNAs were readily transferred to the HOMO orbital of Ru-Py, and the excited electrons in the LUMO orbital were applied for CO_2 reduction. The probable intermediate produced on the Ru-Py/TNTAs photocathode was further detected

by ΔA spectra and GCMS, and the possible reaction pathway for CO_2 methanolization was elaborated.

2. Experimental

2.1. Materials

Titanium foil (99.5%) and $\text{Ru}(\text{bpy})_2\text{Cl}_2$ (99%) were purchased from Aladdin Industrial Inc. Ammonium fluoride (NH_4F , 99.5%), ethylene glycol ($\text{HOCH}_2\text{CH}_2\text{OH}$, 99.5%), sodium hydroxide (NaOH), aqueous ammonia (28%), ethanol (99.8%), N,N-dimethylformamide (DMF, 99.5%), 2,2'-bipyridine (99.5%) and 4-formylbenzoic acid (99.5%) were all analytical reagent and purchased from Sinopharm Chemical Reagent Co., Ltd, SCRC, China.

2.2. Preparation of photocathode

TiO_2 nanotube arrays(TNTAs)substrate electrode was prepared by three steps anodization as the literature report [36]. Titanium foils were polished to a mirror finish before using. Before anodization, the foils were cleaned via ultrasonication in acetone and ethanol successively, followed by drying the samples in the flow of N_2 . Electrochemical anodization was performed using a DC power supply (Sovotek, E5200-3 75 V/2A DC Power Supply, DaHua Electronic, China) in a two electrode configuration with a platinum foil as the counter electrode at 10 °C and 60 V in electrolytes including ethylene glycol with 2.0 vol% H_2O and 0.3 wt% NH_4F . The first and second steps anodization were carried out for 4 h and 2 h respectively to grow TiO_2 NTs layers which was removed by ultrasonication. The third step anodization was carried out for 5 mins. After the anodization process, the samples were rinsed with water,

Table 1

The cathodic current of TNTAs, Ru-Py and Ru-Py/TNTAs in N_2 -saturated and CO_2 -saturated 0.1 M KCl solution with the -1.0 V overpotential.

| $j/mAcm^{-2}$ | N_2 | | | CO_2 | | |
|---------------|-------|-------|-------------|--------|-------|-------------|
| | TNTAs | Ru-Py | Ru-Py/TNTAs | TNTAs | Ru-Py | Ru-Py/TNTAs |
| Light Off | -1.56 | -0.89 | -2.37 | -1.89 | -2.25 | -2.79 |
| Light On | -2.23 | -1.03 | -3.19 | -2.63 | -3.13 | -4.58 |
| Δj | 0.67 | 0.14 | 0.82 | 0.74 | 0.88 | 1.79 |

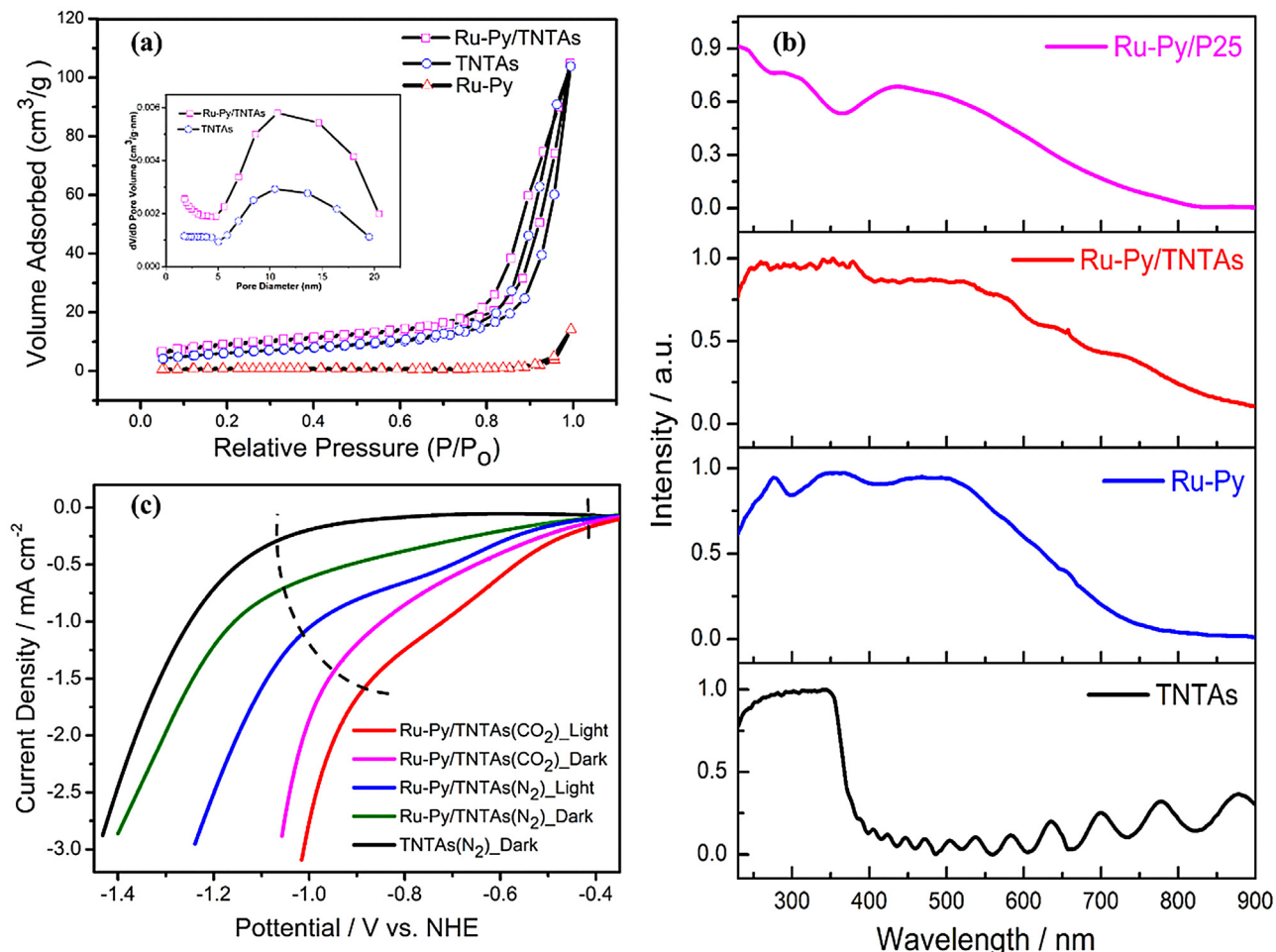


Fig. 3. (a) Nitrogen adsorption-desorption isotherms of Ru-Py, TNTAs and Ru-Py/TNTAs. The illustration was the pore size distributions of TNTAs and Ru-Py/TNTAs; (b) The UV-DRS spectra for Ru-Py, TNTAs, Ru-Py/TNTAs and Ru-Py/P25; (c) The Linear Sweep Voltammetry of Ru-Py/TNTAs electrode in N_2 -saturated and CO_2 -saturated 0.1 M KCl solution with the scan rate of 0.05 V/s under light on/off.

ethanol and then dried in air, followed by heat-treating at 500 °C for 3 h in air.

All the structures of the complexes involving in this article were shown in scheme S1 in supporting information (SI). 4-(2,6-di(pyridin-2-yl)pyridin-4-yl)benzoic acid was obtained following the related procedure [37]: 3.0 g of 4-carboxybenzaldehyde (20 mmol), 5.0 mL 2-acetylpyridine (44 mmol), 16.8 g ammonium acetate, and 25 g acetamide were mixed together and heated to a reflux (~ 130 °C). The solution became dark brown, then red with a precipitate. After 2 h, the reaction mixture was removed from heat, and a separate solution was prepared with 14.4 g NaOH (360 mmol) and 36 mL H_2O . The reaction mixture was cooled with ice, and the NaOH solution was added over the course of 5 min. The solution was then heated to 160 °C for 2 h, followed by addition of 70 mL of H_2O . The yellow precipitate was collected on a Buchner funnel, and washed only once with water (further washes resulted in significant loss of yield). The gooey solid was dissolved in hot H_2O and precipitated out in acetone. This process was repeated until a

light yellow, fluffy solid was collected. Drying in vacuum to give 2.0 g pure compound 4-(2,6-di(pyridin-2-yl)pyridin-4-yl)benzoic acid (40% yield).

Ru-Py was obtained following the related procedure [38,39]: To a solution of $Ru(bpy)_2Cl_2$ (300 mg) in EtOH (5 mL) and DMF (5 mL) was added 4-(2,6-di(pyridin-2-yl)pyridin-4-yl)benzoic acid (105 mg) and water (2 mL). The mixture was stirred at 120 °C for 9 h under the protection of N_2 . The mixture was cooled to room temperature and filtered to give the title compound (Ru-Py) as a dark red solid which was dried in vacuo (120 mg).

Ru-Py/TNTAs Photocathode was prepared as the following description: Ru-Py (10 mg) was added to acetonitrile (50 mL), and then the TNTAs substrate electrodes was added to the above solution. The mixture was heated to 95 °C for at least 8 h under the protection of N_2 to achieve the saturation adsorption. The electrodes was took out, washed with acetonitrile and dried in vacuum at 40 °C to give the Ru-Py/TNTAs photocathode.

Table 2

TON and Faradic efficiency compared to results presented in the literature.

| System | pH | TON | $f_{\text{MeOH}}(\%)$ | $f_{\text{total}}(\%)$ | Referee |
|---|-----|------|-----------------------|------------------------|-----------|
| Ru-Py/TNTAs(PEC) | 5.0 | 62.6 | 63.9 | 93.6 | this work |
| [Ru(phen) ₃] ²⁺ .Py(PC) | 5.1 | 0.33 | 66 | – | 27 |
| [Ru(phen) ₂ (ptpb α)] ²⁺ (PC) | – | 0.4 | 1.1 | – | 46 |
| Ru(bpy) ₂ (PIP) ²⁺ (PEC) | 5.0 | 6.4 | 27.3 | 83.1 | 47 |
| Pt/4-NH ₂ -Py | 5.2 | – | 39 | 51 | 24 |
| Au/Py(EC) | 5.0 | 2.5 | 22 | – | 21 |
| CuInS ₂ /Py (PEC) | 5.2 | 0.16 | – | – | 25 |
| p-GaP/Py (EC) | 5.2 | – | 3.6 | – | 26 |
| Cu/PdH/Py (EC) | 5.2 | – | 15 | – | 26 |
| CdSe/Py (PEC) | 5.0 | – | 0 | 60.7 | 48 |
| Pt/Py (EC) | 5.2 | – | 14.5 | 33 | 49 |

Values calculated based on information given in the reference. TON calculated based on Py catalyst.

Table 3

Methanol Production in Different Condition.

| | Amount (μmol) | TON | Faradic efficiency |
|----------------------------|----------------------------|------|--------------------|
| Ru-Py/TNTAs(PEC) | 84.8 \pm 4.8 | 62.6 | 63.9% |
| Ru-Py/TNTAs(EC) | 24.8 \pm 2 | 16.8 | 14.5% |
| Ru-Py/TNTAs PC(with AA) | 35.9 \pm 1.1 | 23.2 | – |
| Ru-Py/TNTAs PC(without AA) | 1.3 \pm 0.4 | 0.9 | – |
| TNTAs + Py(PEC) | 12.3 \pm 1.1 | 8.3 | 12.2% |
| TNTAs(PEC) | – | – | – |
| Ru-1/TNTAs(PEC) | 41.3 \pm 3.6 | 28.1 | 21.3% |
| Ru-2/TNTAs + Py(PEC) | 17.2 \pm 1.9 | 11.7 | 11.8% |
| Ru-Py(FTO) (PEC) | 27.6 \pm 3.2 | 18.7 | 30.1% |

AA: Ascorbic acid.

2.3. Chemical characterizations

A fluorescence spectrophotometer (Hitachi, F-7000) was employed to characterize the steady-state fluorescence spectra of Ru-Py. ¹H NMR spectra were recorded on a Bruker AVANCCE III 400 MHz spectrometer operating at 400 MHz. The absorption spectra were obtained by an ultraviolet-visible spectrophotometer (UV-vis, Agilent 8453). Methanol was detected with a Thermo GCMS (Thermo Fisher 310 GC system with a TSQ Quantum XLS Mass Selective detector equipped with automatic sampling device) by headspace analysis. Sample aliquots were preheated at 90 °C in a 20 mL headspace vial with a septa cap, and 2.5 mL of the head space gas was injected from a syringe heated to 95 °C and analyzed in the GC-MS instrument.

All PEC measurements were measured using a conventional three-electrode system on a CHI660C electrochemical workstation (CH Instruments, Inc., USA) with the as-prepared electrode as the working electrode, Ag/AgCl (Saturated KCl) as the reference electrode and a platinum sheet as the counter electrode in 0.1 M KCl aqueous solution. All the potentials were referenced to Ag/AgCl unless stated otherwise. To separate the cathode and anode reactions for controlled potential electrolysis of CO₂ reduction, the electrochemical system was composed of a standard two compartment electrolysis cell, and 0.1 M KCl aqueous solution was used as the supporting electrolyte. The amperometric i-t curve was obtained with an interval of 200 s for light on/off under the light intensity of 20 mW cm⁻² at a constant potential of -1.0 V (light Source: LA-410UV, Hayashi, Japan).

2.4. PEC reduction of CO₂ and products detection

The PEC CO₂ reduction was proceeded in a 100 mL homemade double-chamber reactor divided with proton exchange membrane. Typically, 100 mL 0.1 M KCl solution was used as the electrolyte solution for reduction. Before reduction, high purity CO₂ (99.99%) gas was bubbled to the KCl aqueous solution for 40 min at a flow rate of 40 mL/min to remove the dissolved oxygen completely.

Under such condition, CO₂ reached saturation in the electrolyte. The potential during the PEC reduction was kept constant at -0.9 V under 100 mW cm⁻² irradiation (light Source: PLS-SXE300 xenon lamp, Beijing Perfect Light Co., Ltd., China). Note that the ultrapure water with its conductivity reaching 18.2 MΩ cm was used for all the solutions preparation.

A headspace GCMS was used to detect the production of methanol. The chromatographic column (SHRX105MS, 30-m length and 0.5 mm inner diameter) at an oven temperature of 40 °C was employed in combination with a MS detector at 230 °C and helium was the carrier gas. Detection at m/z =31 was chosen to identify methanol as the reaction products. The samples were preheated at 90 °C in a 20 mL headspace vial with a septa cap, and 1.0 mL of the head space gas was injected from a syringe heated to 90 °C and analyzed in the GC/MS instrument. Control samples containing known concentrations of methanol (in the range 40 – 280 mM) were analyzed to obtain a standard curve. Techcomp GC7000 (Techcomp, China) gas chromatogram equipped with thermal couple detector (TCD) and 5 Å molecular filled column was employed to exam methane, CO and other gaseous product. Nash's reagent method was used to detect the production of formate acid and formaldehyde in the aqueous phase. Nash reagent was prepared by the following procedure: 25.0 g of ammonium acetate, 2.1 mL of acetic acid and 0.2 mL of acetylacetone was added to water and making the total volume of the solution 100 mL. The detection for formaldehyde and formate acid as the following processes: 2.0 mL of liquid sample was mixed with 2.0 mL of Nash reagent and shaken for 1 h at 60 °C. The final solution was analyzed by UV-vis spectroscopy and the absorbance at 413 nm was used to quantitate the amount of formaldehyde. Magnesium powder (50 mg) was added to 0.5 mL of liquid sample, following by drop-wise addition of 0.5 mL 37% hydrochloric acid (10 M) at 0 °C and then 3 mL 1 M sodium hydroxide. The resultant suspension was centrifuged at 10 000 rpm for 3 min and 2 mL of supernatant was mixed with 2 mL of Nash reagent and shaken for 1 h at 60 °C for UV-vis analysis (413 nm) to determine the amount of formic acid (Nash's method).

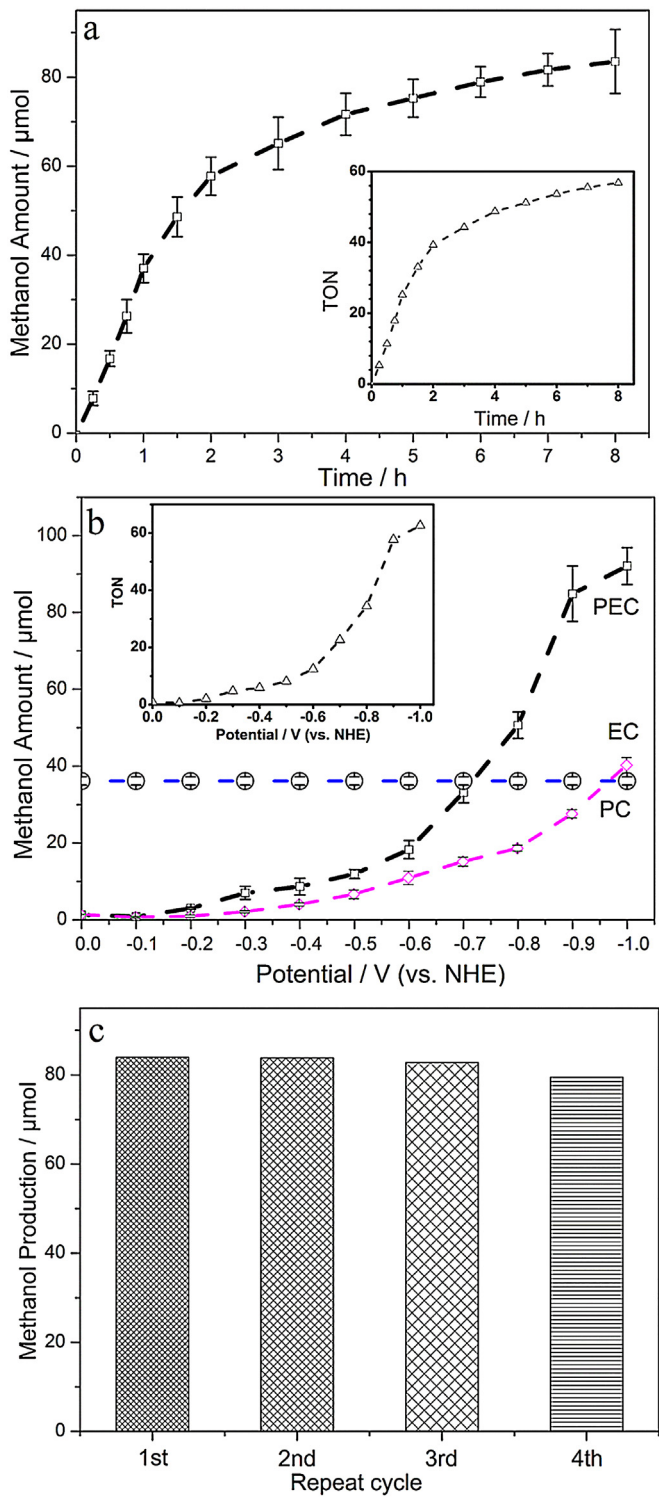


Fig. 4. (a) Product amount and TON growth of methanol with different potential for Ru-Py/TNTAs; (b) Product amount and TON growth of methanol with different irradiation time for Ru-Py/TNTAs; (c) The PEC four cycles methanolization production for the stability measurement of Ru-Py/TNTAs.

3. Results and discussion

3.1. Physical and photoelectrochemical property of the Ru-Py/TNTAs photocathode

The morphologies of the synthesized samples were revealed by scanning electron micrographs (SEM) as shown in Fig. 1 (a–d).

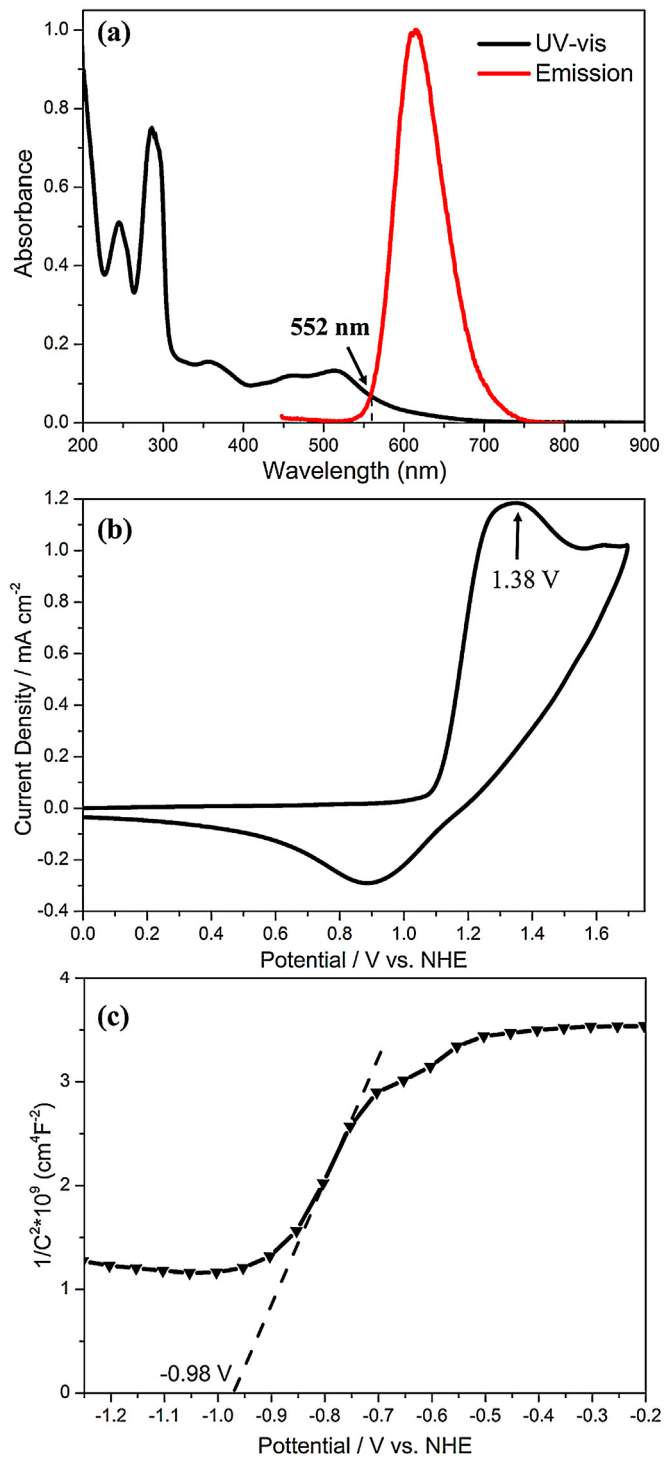


Fig. 5. (a) The UV-vis Spectra and photoluminescence spectra of 0.05 M Ru-Py in CH₃CN solution; (b) CVs in DMF/1.0 M H₂O with 0.1 M (n-Bu₄N)(PF₆) as supporting electrolyte; (c) Mott-Schottky plot for the conduction band of Ru-Py by investigating the relationship between impedance and potential change at a fixed frequency in 0.1 M KCl at pH = 7.0.

The surface of TNTAs with uniform mesh structure was quite smooth before Ru-Py was loaded and the pore diameter was about 60 nm. After Ru-Py was combined to the semiconductor electrode, the surface of TNTAs became extremely rougher. It indicated the metal-organic molecular catalyst was fixed on the semiconductor electrode uniformly. The average tube length decreased to only about 450 nm (Fig. 1d). It is worth mentioning that the ordered

TNTAs possessing large porosity were rationally synthesized onto substrate electrode, which was highly favorable for uniform deposition of metal-organic complex onto the surface of substrate electrode and the side wall of the pores.

The X-ray diffraction patterns of bare TNTAs and Ru-Py loaded TNTAs catalysts in Fig. 1e presents similar crystallinity. The Ru-Py has no obvious diffraction peaks while there are six diffraction peaks appearing at $2\theta = 25.26^\circ, 37.77^\circ, 47.98^\circ, 53.88^\circ, 54.01^\circ, 62.70^\circ$ and 68.86° which corresponded to (101), (004), (200), (105), (211), (204) and (116) planes of typical anatase TiO_2 [40,41]. The crystallinity didn't change after the Ru-Py fixing on the surface of TNTAs.

To further characterize the fixing of Ru-Py on TNTAs, the Raman spectra was employed to record the changes of TNTAs before and after Ru-Py loaded. As shown in Fig. 1f, the characteristic bands of anatase TiO_2 are observed obviously at 153, 197, 397, 519 and 640 cm^{-1} . The backbone peaks in the $1250 - 1600\text{ cm}^{-1}$ range can be related to the C–C and C=N stretching vibration in the polypyridine skeleton while the 1170 and 1014 cm^{-1} peaks belonged to the C–H bending vibration of the ligand. The weak vibration peaks in the $220 - 530\text{ cm}^{-1}$ range can be related to the Ru–N stretching mode of polypyridine complexes. Compared with the Raman spectra of pure TNTAs and Ru-Py, all the vibration peaks of TNTAs and Ru-Py were reflected on the prepared photoelectrocathode which indicated that Ru-Py was successfully loaded on the TNTAs substrate electrodes.

The presence of the prepared Ru-Py complex on the photocathode surface was further confirmed by X-ray photoelectron spectroscopy (XPS) measurements, which showed a clearly visible signal for Ru(II) at 280.4 eV , in agreement with previously reported values [42,43]. The binding energy of Ru(II) $3p_{3/2}$ at 464.6 eV and 282.3 eV are overlapped with $\text{Ti}2p_{1/2}$ and C 1s respectively [44,45]. Ru(III) was not detected with the binding energy at 282 eV which indicated no other phases of the Ru complex were discerned. Additionally, nitrogen, carbon and titanium as well as oxygen could also be confirmed (Fig. 2). Moreover, The N 1s XPS spectrum displayed two peak components at 401.2 and 399.2 eV due to C=N and C–N of bipyridine which further confirmed the presence of the Ru(II) complex.

Fig. 3a exhibits the N_2 adsorption-desorption isotherms of TNTAs, Ru-Py/TNTAs and Ru-Py samples. The BET surface area of TNTAs was $56.03\text{ m}^2\text{ g}^{-1}$ while the Ru-Py power was only $4.16\text{ m}^2\text{ g}^{-1}$. It was notable that the BET surface area of TNTAs was increased to $71.55\text{ m}^2\text{ g}^{-1}$ after Ru-Py was loaded. Similarly, BJH adsorption pore volume increased from $0.025\text{ cm}^3\text{ g}^{-1}$ to $0.030\text{ cm}^3\text{ g}^{-1}$ while pore diameter decreased from 26.0 nm to 19.9 nm with Ru-Py loading which may be attributed to the Ru(II) complex inset into the hole of TNTAs.

Diffuse reflectance UV-vis spectra (DRS) were recorded to investigate the influence of Ru-Py on the optical property of TNTAs. As shown in Fig. 3b, TNTAs photoelectrode exhibited a pronounced adsorption band in the visible light region due to its unique periodic porous layer structure (photonic crystal layer). The Ru(II) organic-inorganic complex molecular catalyst exhibited broad visible absorption due to the excellent $\pi-\pi^*$ conjugation of the polypyridine ligand and the metal-ligand electron transition. Compared with Ru-Py/P25, the absorption band edge of the Ru-Py modified TNTAs photoelectrode exhibited a 90 nm red-shift, which may be due to the outstanding visible optical absorption properties of TNTAs. The corrugate absorption edge of DRS in the range from 600 nm to 900 nm indicated the periodic porous layer structure was maintained, but the absorption intensity was reduced, due to the presence of the Ru-Py on the surface of TNTAs.

In order to testify the CO_2 reduction capability, the EC and PEC behavior of Ru-Py/TNTAs in CO_2/N_2 saturated 0.1 M KCl solution was investigated. As shown in Fig. 3c, the dark cathodic current on Ru-Py/TNTAs remarkably increased in CO_2 -saturated solution

compared with that in N_2 -saturated solution attributed to the EC CO_2 reduction. Under the simulation solar irradiation, the cathodic photocurrent on Ru-Py/TNTAs in CO_2 -saturated solution further increased, and the onset potential for CO_2 reduction was positively shifted to -0.52 V . It indicated that the light irradiation took a significance role for CO_2 reduction owing to the photo-sensitization effect of the coaction between Ru-Py and TNTAs.

The photocurrent response of Ru-Py/TNTAs in 0.1 M KCl electrolyte solution originated from the unique PEC performance and optical absorption properties of the as-prepared Ru-Py/TNTAs photocathode. The optimized PEC performance of the as-prepared photocathodes was presented in Table 1 and Fig. S1 (SI) at -0.9 V (vs. NHE) with chopped light irradiation (200 s). The cathodic current of Ru-Py was detected by loading Ru-Py on the surface of FTO as working electrode. In N_2 -saturated solution, the current of TNTAs, Ru-Py/FTO and Ru-Py/TNTAs electrode were all obvious increased after irradiation due to their respective light absorbance. Meanwhile, the added current value (Δj) of Ru-Py/TNTAs photocathode with light off/on was equal to the summation of Ru-Py and TNTAs approximately which indicated the Ru-Py/TNTAs photocathode did not depress the two components' light harvesting property. Compared with that in N_2 -saturated solution, the Δj of Ru-Py in CO_2 -saturated solution was added from 0.14 mA cm^{-2} to 0.88 mA cm^{-2} while that of TNTAs was only changed from 0.67 mA cm^{-2} to 0.74 mA cm^{-2} . It may be attributed to the higher reduction capacity of Ru-Py than TNTAs. In CO_2 -saturated solution, the Δj on Ru-Py/TNTAs photocathode was about 2 times higher than that in N_2 -saturated solution, which showed an efficient CO_2 reduction on Ru-Py/TNTAs. The Δj of Ru-Py/TNTAs (1.79 mA cm^{-2}) was higher than the summation of TNTAs (0.74 mA cm^{-2}) and Ru-Py/FTO (0.88 mA cm^{-2}), which indicated the composite electrode exhibited more excellent CO_2 PEC reduction property than the two pure components.

3.2. PEC performance for CO_2 reduction

The heterogeneous PEC CO_2 reduction performance was conducted in 100 mL of CO_2 -saturated 0.1 M KCl aqueous solution under solar light irradiation at -0.9 V (vs. NHE). In the final aqueous solution, formic acid and methanol were detected the liquid products after 8 h PEC CO_2 reduction, while methane, CO and other gas products were not detected. The yield of methanol was noticeable though formic acid was the primary competitive reduction product in the reaction. The Faradaic efficiency (η) and TON was obtained from the following equations:

$$\eta = (m_p \times n \times F) / (I \times t) \quad (1)$$

$$\text{TON} = m_p / m_{\text{cat}} \quad (2)$$

where m_p is product amount (mol), n is transferred number of electrons, F is Faraday constant ($96485.34\text{ C mol}^{-1}$), I is total observed current (A), t is reaction time (s) and m_{cat} is catalyst quantity (mol).

As the desired product, the methanol produced was $84.8\text{ }\mu\text{mol}$ with a TON of 62.6 and a faradaic efficiency of 63.9% under PEC condition for 8 h as shown in Fig. 4a. The value was much higher than that obtained from pure electrochemical ($24.8\text{ }\mu\text{mol}$) and photocatalytic reduction methods ($35.9\text{ }\mu\text{mol}$). Furthermore, $103.6\text{ }\mu\text{mol}$ formic acid was also detected with a faradaic efficiency of 27.1% . The selectivity for methanol was 45.0% and the total faradaic efficiency reached 93.6% . As shown in Table 2, to further evaluate the CO_2 reduction performance of Ru-Py/TNTAs, a comparing of the CO_2 reduction performance with literature reports are summarized. As we can see, the TON or faradaic efficiency for methanol was quite higher than most reported systems under photo/electrode condition with pyridium catalyst [21,24–27,46–49]. The faradaic efficiency for methanol on our PEC system is comparable to that

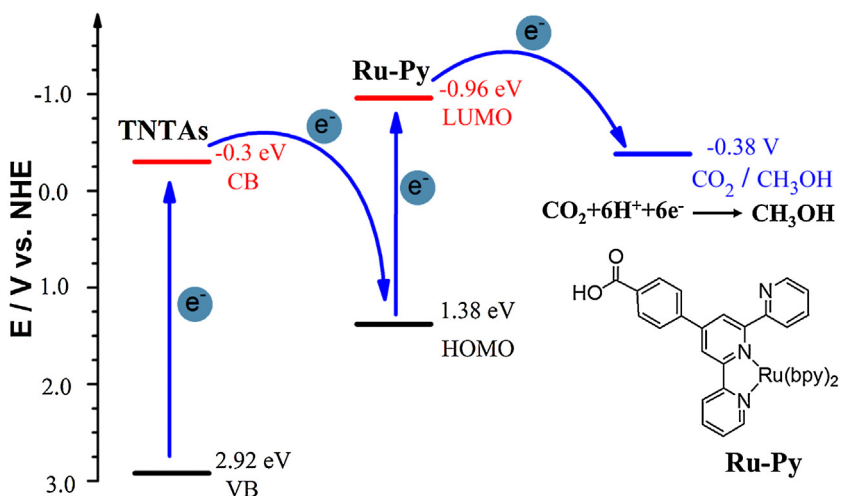


Fig. 6. Energy levels positions of the Ru-Py HOMO-LUMO orbital and the redox potentials of CO_2 .

on some noble metal based EC system like Au/Py [21] and Pt/4-NH₂-Py [24] as well as on heterogeneous semiconductor/Py or molecular catalyst PEC systems like CuInS₂/Py [24], CdSe/Py [48] and Ru(bpy)₂(PIP)²⁺ [47].

To evaluate the contribution of PC and EC, three parallel reactions were introduced (As shown in Table 3 and Fig. 4b). The In PC system, 35.9 μmol methanol (TON: 23.2) was obtained with 0.1 M ascorbic acid (AA) as electron donor while only 1.3 μmol methanol (TON: 0.9) was detected in the absence of AA, indicating the plentiful electron supplement was crucial for the CO_2 reduction. It also indicated AA can easier supplied plentiful electron for CO_2 reduction than water. Under EC CO_2 reduction system, the methanol production had gradual increase following the potential added from 0 to -1.0 V , however, the EC methanol production was much lower than PEC. In EC CO_2 reduction system, only 24.8 μmol methanol (TON: 16.8, Faradaic efficiency: 14.5%) was detected at -0.9 V . It suggested that the prepared Ru-Py/TNTAs cathode was a better photocatalyst rather than an electrocatalyst. We could also find that the methanol production under PEC condition was higher than the total amount of PC condition with AA as electron donor and EC condition at -0.7 V , which suggested the excellent synergistic effect for CO_2 reduction between photocatalysis and electrocatalysis. Under PEC condition, the electrode not only catalyzed the EC conversion of CO_2 directly under the assistance of light irradiation, but also functioned as electron source for PC CO_2 conversion. The two roles increased the electron utilization efficiency which further increased the methanol production.

The linking groups such as carboxyl and phosphate group took crucial affection in the constitution of metal oxide overlayers substrate and organic molecules for fast electron migration [28,50–52]. To confirm the effect of carboxyl group's linking, Ru-Py was esterified by 4 M HCl/methanol for 2 h at room temperature to give a non-carboxyl Ru(II) complex (Ru-1, the structure of Ru-1 was shown in Scheme S1). The Ru-1/TNTAs photoelectrocathode produced only 41.3 μmol methanol under 8 h irradiation at -0.9 V . This may be caused by the repressed electron transfer from TNTAs to Ru(II) complex without carboxyl group's linking, thereby the methanol production was reduced. In other words, the electron in TNTAs substrate electrode migrated to the HOMO orbital of Ru-Py, which reduced the photoinduced electron-hole pair recombination of TNTAs. The electron from TNTAs was further used for CO_2 reduction at the pyridyl catalytic unit.

Connecting the organic or metal-organic catalyst to semiconductor photocathodic or photosensitizer with appropriate chemical bonding was a fairly effective method to improve the electron

transfer, thus increase the catalytic efficiency [27,53,54]. The intermolecular electron migration from photosensitizer to catalyst become intramolecular migration due to the connection of chemical bonding. On the Ru-Py/TNTAs photocathode, a pyridyl catalytic unit was covalently bonded on the Ru(II) photosensitizer by C–C single bond. To investigate the role of the chemical bonding between Ru(II) photosensitizer and pyridyl catalytic unit, a photocathode (Ru-2/TNTAs) containing Ru (II) complex photosensitizer without pyridyl unit was prepared for CO_2 PEC reduction. In CO_2 -saturated 0.1 M KCl aqueous solution, only 17.2 μmol methanol was detected under 8 h PEC reduction with the present of 0.05 M pyridine. The methanol production was much lower than Ru-Py/TNTAs photocathode (84.8 μmol). It indicated the intramolecular electron transfer was more efficient than that intermolecular.

The contribution of TNTAs substrate electrode, Ru(II) photosensitizer and pyridine catalyst for PEC CO_2 reduction was further investigated by designed comparison experiments as list in Table 3. Without Ru-Py, the TNTAs with pyridine in PEC process produced only 12.3 μmol methanol, indicating the Ru(II) photosensitizer played an important role in enhancing the light absorption in visible region, resulting in improved light harvest and methanol production. But, there was no methanol detected with pure TNTAs, further indicating the exposed pyridyl unit was the pivotal catalytic sites for methanol production. Without TNTAs, the pure Ru-Py/FTO who had a Ru(II) photosensitizer and pyridyl catalytic unit contributed 17.2 μmol methanol under PEC condition indicated the TNTAs can promote the methanol production. It may attributed to the TNTAs can supply abundant electrons to Ru-Py for CO_2 reduction under PEC condition. In addition, as shown in Fig. S2, the methanol production was proportional to the Ru(II)-Pyridyl complex loading amount and then tended to be a plateau. It also indicated the Ru-Py took important role for the methanol production indirectly.

As shown in Fig. 4b, the potential dependent PEC CO_2 reduction was involved to further estimate the contribution of EC process. From -0.1 V to -1.0 V , the methanol production was increasing accompanied with the potential added. At the potential of -0.7 V , the methanol production was equal in general to the PC process with AA as electron donor. This indicated the -0.7 V potential offered the equal amount of electron as electron donor. Meanwhile, under the potential less than -0.7 V the bias potential only functioned as electron donor source for PC process. As the potential exceeding to -0.7 V , the EC process not only functioned as electron donor for PC process, but also catalyzed CO_2 reduction directly. By comparison of the PEC process at -0.9 V and -1.0 V , the added amount of methanol was only 7.2 μmol after 8 h which may be

due to the hydrogen evolution reaction (HER) occurring rapidly at -1.0 V . As shown in Fig. S3, the GC detected H_2 production from -0.8 V to -1.0 V increased quickly. At -0.8 V , no H_2 was detected, but the amount soared to $100\text{ }\mu\text{mmol}$ at -1.0 V . As the competing reaction, HER immensely suppressed the CO_2 reduction after the potential reached hydrogen-evolution condition.

A recycling experiment of PEC CO_2 reduction to methanol on Ru-Py/TNTAs was investigated to evaluate the stability of the photoelectrocathode material. In order to examine the reproducibility in every 8 h , the Ru-Py/TNTAs photoelectrocathode was drawn from the 0.1 M KCl solution, and rinsed with distilled water. Then it was used for the next run reaction. As shown in Fig. 4c, the four time cycles methanol production based on the peaks area of GCMS at 1.352 min ranged from 79.50 to $83.95\text{ }\mu\text{mol}$ which indicated the Ru-Py/TNTAs had good stability in the PEC CO_2 reduction. As shown in Fig. S4, the SEM images was recorded to characterize the morphology of Ru-Py/TNTAs before and after CO_2 reduction for 4 cycles. The TNTAs kept extremely rougher surface which indicated the metal-organic molecular catalyst still loaded on the semiconductor electrode after 4 cycles experiment. The XRD spectra also indicated the photocathode after 4 cycles was accorded with the prime state before CO_2 reduction.

3.3. Probable reaction route for PEC CO_2 conversion to methanol

To investigate the probable electron transfer route during the CO_2 reduction process, the band alignment of Ru-Py/TNTAs was discussed. The HOMO-LUMO orbital energy level of Ru-Py was estimated according to the literatures [55–57]. As a classical metal-organic complex, the electron can migrate in the whole molecule as shown in Fig. 5a. The intense absorption bands of the UV-vis absorption spectrum at 240 nm can be assigned to the spin-allowed intra ligand ($n-\sigma^*$) transitions while 300 nm attributed to the $\pi-\pi^*$ transitions of the conjugated ligand. The broad band at lower energy in the 380 – 450 nm region was attributed to the d(Ru)- π^* (diimine) metal-to-ligand charge-transfer (MLCT) transitions. The Ru(II) complex showed remarkable photoluminescence properties under the excitation of 397 nm wavelength light stimulation and the maximum emission peak laid at 625 nm . Based on the wavelength intersection of normalized UV-vis and photoluminescence spectra, the energy gap of Ru-Py was obtained as 2.22 eV . The HOMO orbital energy which was equals to the Ru^{III/II} redox potential (E_{ox} vs NHE) approximatively, was estimated as 1.38 V from CVs in 0.05 mM Ru-Py DMF solution with $n\text{-Bu}_4\text{NPF}_6$ (0.1 M) as supporting electrolyte just as shown in Fig. 4b. Then the LUMO orbital energy of Ru-Py was calculated to be -0.96 V . The Mott-Schottky method was further investigated to detect the LUMO orbital energy directly in 0.1 M KCl (as shown in Fig. 5c). We could find that the LUMO orbital energy of Ru-Py was approximately -0.98 V (vs. NHE) which was equal to the value obtained from UV-vis/CVs measurement technique. As literature reported, the more negative CB or LUMO orbital energy the more efficient for CO_2 reduction [58]. The results indicated Ru-Py could provide adequate driving force for CO_2 reduction owing to the more negative LUMO orbital energy (-0.96 V) than $\text{CO}_2/\text{methanol}$ potential (-0.38 eV). The energy band alignment of Ru-Py/TNTAs was illustrated in Fig. 6. Upon light irradiation, two process may be involved concerning the electron transfer in Ru-Py/TNTAs. One was that the photogenerated electrons on the conduction band of TNTAs were transferred to the HOMO orbital of Ru-Py, and the excited electrons in the LUMO orbital were applied for CO_2 reduction (Process I). The other is that the excited electrons in the LUMO orbital were transferred to the conduction band of TNTAs and CO_2 was reduced (Process II). The PEC CO_2 reduction results listed in Table 3 showed that there was not methanol was detected on pure TNTAs. This results indicated that the electron transfer must follow process I [59,60]. As shown

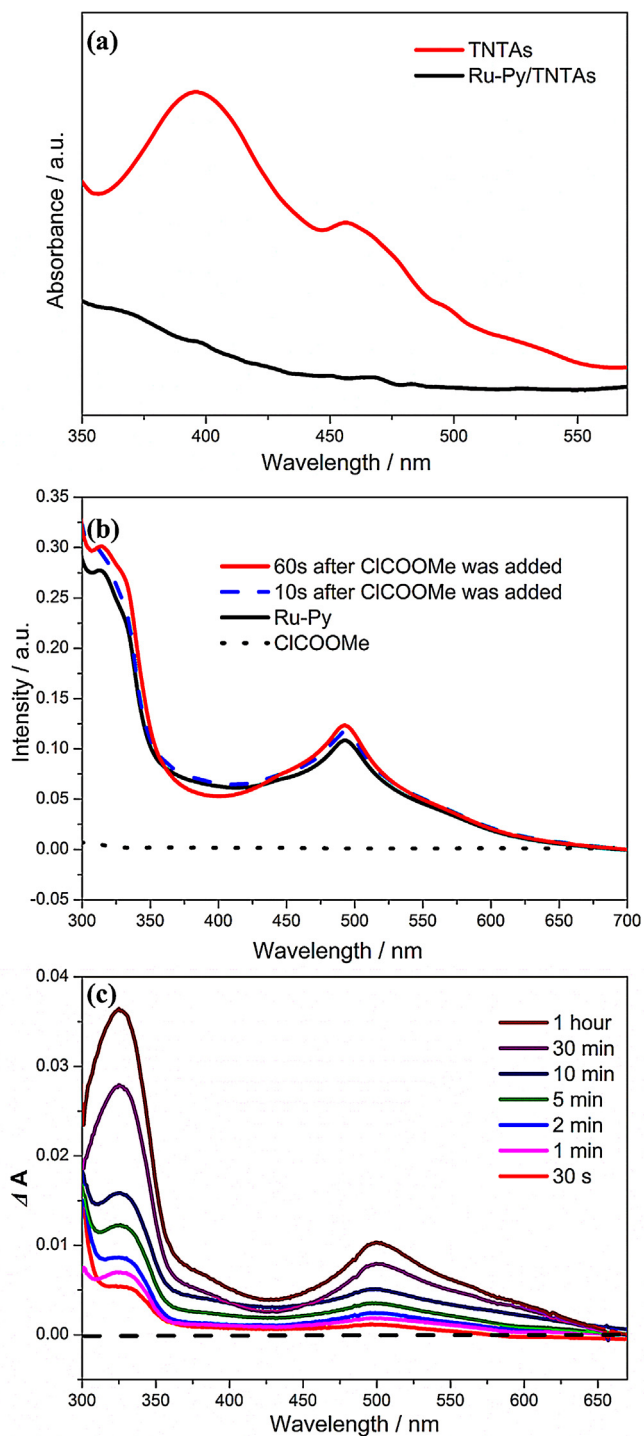
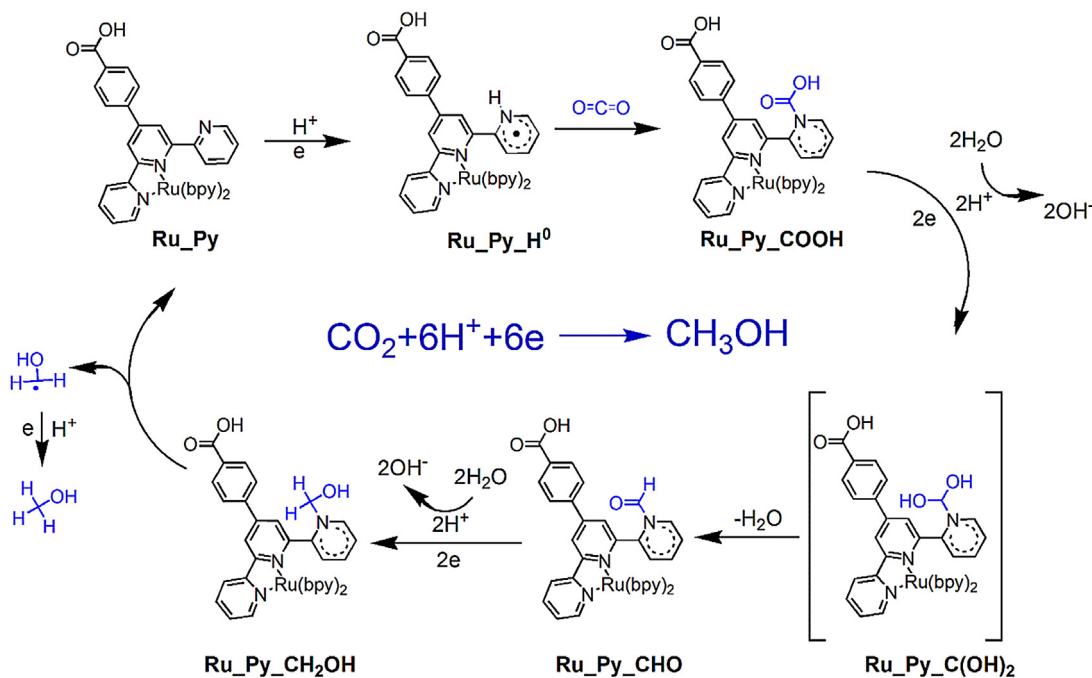


Fig. 7. (a) The photoluminescence spectra of TNTAs and Ru-Py/TNTAs; (b) UV-vis absorption spectrum of Ru-Py acetonitrile solution, 5s after the addition methylic chloroformate (10 equiv), 60s after the addition of methylic chloroformate; (c) ΔA spectra of Ru-Py ($10\text{ }\mu\text{M}$) during PEC system in CO_2 saturated 0.1 M KCl aqueous solutions.

in Fig. 6, the electron transfer followed the Z-scheme style due to that the TNTAs CB (-0.3 V) lay more negative than HOMO orbital of Ru-Py provided enough driving force for CO_2 reduction [50]. In this situation, the exposed pyridyl in Ru(II) complex was presumed as the active catalytic sites in the methanol production.

In order to further confirm the migration of photogenerated electrons in Ru-1/TNTAs, photoluminescence (PL) spectra was introduced to record the fluorescence of Ru-Py/TNTAs (Fig. 7a).

Scheme 1. Proposed reaction pathway for PEC CO_2 reduction.

With the excited wavelength of 310 nm, TNTAs exhibited a wide and strong PL signals in the range of 350 – 500 nm. However, the fluorescence of TNTAs nearly disappeared after Ru-Py immobilized. The reduced PL intensity is possibly due to the efficient photo-generated electron-hole pair separation on the TNTAs surface by injection of the electrons on the conduction band of TNTAs to the HOMO orbital of Ru-Py through the covalent bonds [59–62]. As a result, the photoactivity of TNTAs and photostability of Ru-Py were simultaneously improved due to the charge transfer mode.

Based on the others report and our previous research, the protonation of pyridyl ($Ru-Py-H^0$) was the first step for CO_2 reduction at weakly acidic condition as shown in Scheme 1 [19,47]. Then CO_2 was inserted to the N–H bond of $Ru-Py-H^0$ to give the pivotal pyridiniumformate intermediate ($Ru-Py-COOH$). To verify the formation pyridiniumformate during the reduction process, a simulate reaction was conducted as follows. Methyl chloroformate which does not display absorbance at 300 – 800 nm in acetonitrile solution (the dash line in Fig. 7b) was employed to simulate the pyridiniumformate because it can react conveniently with the exposed N atom in pyridyl to give the pyridiniumformate spontaneously without any further processing. As well known, the absorption of UV-vis spectra mainly caused by the conjugation π electrons in ligand. Hence, the absorbance change of the UV-vis spectra at 300 nm – 550 nm after the addition of the methyl chloroformate can be attributed to the generation of pyridiniumformate. As shown in Fig. S5, Ru-2 who had no exposed pyridyl showed no UV-vis spectra changing before and after methyl chloroformate adding. The comparative experiment further proved the exposed N atom in pyridyl acted the key role in the pyridiniumformate formation. The ΔA spectra was employed to record the absorption changes which reflect the formation of pyridiniumformate intermediate during the CO_2 reduction process (as shown in Fig. 7c). The absorbance of the CO_2 saturated aqueous solution was selected as baseline, and meanwhile, the upward counterparts corresponded to new bands appearing due to photolysis. As the pyridiniumformate intermediate generated, the π electrons in C=O double bond conjugate with the ligand of Ru-Py. Therefore, the changes of the UV-vis absorption from 320 nm to 520 nm was caused by the for-

mation of pyridiniumformate intermediate by the C–N bond which was composed of the C atom from CO_2 and N atom from pyridyl. The variation tendency of the ΔA spectra was in accordance with the result of the above simulate reaction. Besides, the time-dependent change of the ΔA spectra showed the pyridiniumformate increased continually [63], which was consistent with the methanol production within the same time scale.

To further illustrate the process of PEC CO_2 reduction to methanol, GCMS was employed to detect the probable intermediate. In a CO_2 -saturated dichloromethane solution containing 0.05 M Ru-Py, 30 min PEC CO_2 reduction with GC electrode as working electrode was performed before GCMS analysis. Mass spectrum indicated that two fragment peaks were detected with nuclear cytoplasmic ratio (m/z^+) 398 and 399 as shown in Fig. S6 (SI). The two fragment peaks should correspond with the structure of the intermediate ($Ru-Py-CHO$ and $Ru-Py-CH₂OH$) respectively as shown in Scheme 1. The structure of $Ru-Py-COOH$ and $Ru-Py-C(OH)₂$ were not detected due to their instability under such condition. Finally, $Ru-Py-CH₂OH$ released the methylene-hydroxyl radical who accepted one electron and proton to give methanol. Simultaneously, Ru-Py was regenerated with the generation of the reduction product. Based on the above information, the PEC CO_2 methanolization probably took place following the 6 electron and 6 proton process shown in Scheme 1.

4. Conclusion

In summary, the heterogeneous photoelectrocatalyst was prepared for efficient CO_2 methanolization by covalent immobilization of Ru(II) metal-organic complex containing an exposed pyridyl on TNTAs semiconductor substrate electrode. It further illustrated the prepared catalyst was equipped with excellent photocatalytic activity. The methanol production on the prepared Ru-Py/TNTAs was much higher than that without pyridyl catalytic unit system, indicating the pyridyl CO_2 reduction unit as the key component for CO_2 methanolization. The covalent linking system showed better efficiency in CO_2 methanolization compared with that without covalent linking, which demonstrated the carboxyl covalent link-

ing benefit for electron transfer between the Ru(II) metal-organic complex and semiconductor electrode. Besides, the probable reaction mechanism for PEC CO₂ methanolization was proposed based on intermediate detection by ΔA spectra and GCMS. This article not only provides a new means to link organic heterocyclic molecular catalytic unit, metal-organic complex photosensitizer and semiconductor photocathodic uniform for CO₂ methanolization, but also it supplies a useful way for converting homogenous organic molecule catalyst to heterogeneous catalyst. Therefore, this work could lead to a new opportunity for efficient utility method in carbon resource recycling.

Conflict of interest

The authors declare no competing financial interest.

Acknowledgements

This work was financially supported by the National Natural Science Foundation of China (NSFC, No. 21477085, 21537003) and Science &Technology Commission of Shanghai Municipality (14DZ2261100).

Appendix A. Supplementary data

Supplementary data associated with this article can be found, in the online version, at <http://dx.doi.org/10.1016/j.apcatb.2017.03.060>.

References

- J.L. White, M.F. Baruch, J.E. Pander, Y. Hu, I.C. Fortmeyer, J.E. Park, T. Zhang, K. Liao, J. Gu, Y. Yan, T.W. Shaw, E. Abelev, A.B. Bocarsly, *Chem. Rev.* 115 (2015) 12888–12935.
- S. Gao, Y. Lin, X. Jiao, Y. Sun, Q. Luo, W. Zhang, D. Li, J. Yang, Y. Xie, *Nature* 529 (2016) 68–71.
- J. Ding, Y. Bu, M. Ou, Y. Yu, Q. Zhong, M. Fan, *Appl. Catal. B-Environ.* 202 (2017) 314–325.
- E.E. Benson, C.P. Kubiak, A.J. Sathrum, J.M. Smieja, *Chem. Soc. Rev.* 38 (2009) 89–99.4.
- A.M. Appel, J.E. Bercaw, A.B. Bocarsly, H. Dobbek, D.L. DuBois, M. Dupuis, J.G. Ferry, E. Fujita, R. Hille, P.J.A. Kenis, C.A. Kerfeld, R.H. Morris, C.H.F. Peden, A.R. Portis, S.W. Ragsdale, T.B. Rauchfuss, J.N.H. Reek, L.C. Seefeldt, R.K. Thauer, G.L. Waldrop, *Chem. Rev.* 113 (2013) 6621–6658.
- G.P. Gao, Y. Jiao, E.R. Waclawik, A.J. Du, *J. Am. Chem. Soc.* 138 (2016) 6292–6297.
- V. Jeyalakshmi, R. Mahalakshmy, K.R. Krishnamurthy, B. Viswanathan, *Catal. Today* 266 (2016) 160–167.
- E. Kecsenovity, B. Endrodi, Z. Papa, K. Hernadi, K. Rajeshwar, C. Janaky, *J. Mater. Chem. A* 4 (2016) 3139–3147.
- D. Hursan, A. Kormanyos, K. Rajeshwar, C. Janaky, *Chem. Commun.* 52 (2016) 8858–8861.
- E.M. Fiordaliso, I. Sharafutdinov, H.W.P. Carvalho, J.D. Grunwaldt, T.W. Hansen, I. Chorkendorff, J.B. Wagner, C.D. Damsgaard, *ACS Catal.* 5 (2015) 5827–5836.
- Q. Zhang, C.F. Lin, B.Y. Chen, T. Ouyang, C.T. Chang, *Environ. Sci. Technol.* 49 (2015) 2405–2417.
- P. Kumar, C. Joshi, N. Labhsetwar, R. Boukherroub, S.L. Jain, *Nanoscale* 7 (2015) 15258–15267.
- J.C. Calderona, G. Garcia, L. Calvillo, J.L. Rodriguez, M.J. Lazaro, E. Pastor, *Appl. Catal. B-Environ.* 165 (2015) 676–686.
- M. Lessio, C. Riplinger, E.A. Carter, *Phys. Chem. Chem. Phys.* 18 (2016) 26434–26443.
- S.B. Wang, W.S. Yao, J.L. Lin, Z.X. Ding, X.C. Wang, *Angew. Chem. Int. Ed.* 53 (2014) 1034–1038.
- S.B. Wang, X.C. Wang, *Angew. Chem. Int. Ed.* 55 (2016) 2308–2320.
- S.B. Wang, X.C. Wang, *Appl. Catal. B: Environ.* 162 (2015) 494–500.
- T.E. Rosser, C.D. Windle, E. Reisner, *Angew. Chem. Int. Ed.* 55 (2016) 7388–7392.
- Y. Yan, E.L. Zeitler, J. Gu, Y. Hu, A.B. Bocarsly, *J. Am. Chem. Soc.* 135 (2013) 14020–14023.
- D. Sieh, D.C. Lacy, J.C. Peters, C.P. Kubiak, *Chem. Eur. J.* 21 (2015) 8497–8503.
- A.J. Lucio, S.K. Shaw, *J. Phys. Chem. C* 119 (2015) 12523–12530.
- M. Lessio, E.A. Carter, *J. Am. Chem. Soc.* 137 (2015) 13248–13251.
- T.P. Senftle, M. Lessio, E.A. Carter, *Chem. Mater.* 28 (2016) 5799–5810.
- E.E.B. Cole, M.F. Baruch, R.P. L'Esperance, M.T. Kelly, P.S. Lakkaraju, E.L. Zeitler, A.B. Bocarsly, *Top. Catal.* 58 (2015) 15–22.
- J.L. Yuan, L. Zheng, C.J. Hao, *RSC Adv. 4* (2014) 39435–39438.
- E.E. Barton, D.M. Rampulla, A.B. Bocarsly, *J. Am. Chem. Soc.* 130 (2008) 6342–6344.
- D.J. Boston, Y.M. Pachon, R.O. Lezna, N.R. de Tacconi, F.M. MacDonnell, *Inorg. Chem.* 53 (2014) 6544–6553.
- M. Schreier, J.S. Luo, P. Gao, T. Moehl, M.T. Mayer, M. Gratzel, *J. Am. Chem. Soc.* 138 (2016) 1938–1946.
- K. Maeda, R. Kuriki, O. Ishitani, *Chem. Lett.* 45 (2016) 182–184.
- J.Q. Chen, K.F. Wu, B. Rudshteyn, Y.Y. Jia, W.D. Ding, Z.X. Xie, V.S. Batista, T.Q. Lian, *J. Am. Chem. Soc.* 138 (2016) 884–892.
- C.M. Li, S.T. Zhang, B.S. Zhang, D.S. Su, S. He, Y.F. Zhao, J. Liu, F. Wang, M. Wei, D.G. Evans, X. Duan, *J. Mater. Chem. A* 1 (2013) 2461–2467.
- M. Tahir, N.S. Amin, *Appl. Catal. B-Environ.* 162 (2015) 98–109.
- L.J. Liu, H.L. Zhao, J.M. Andino, Y. Li, *ACS Catal.* 2 (2012) 1817–1828.
- K. Maeda, K. Ishimaki, Y. Tokunaga, D.L. Lu, M. Eguchi, *Angew. Chem. Int. Ed.* 55 (2016) 8309–8313.
- X. Chen, A. Selloni, *Chem. Rev.* 114 (2014) 9281–9282.
- Y. Zhang, B. Tang, Z. Wu, H. Shi, Y. Zhang, G. Zhao, *Green Chem.* 18 (2016) 2424–2434.
- P. Jarosz, P. Du, J. Schneider, S.H. Lee, D. McCamant, R. Eisenberg, *Inorg. Chem.* 48 (2009) 9653–9663.
- J. Ettedgui, Y. Diskin-Posner, L. Weiner, R. Neumann, *J. Am. Chem. Soc.* 133 (2011) 188–190.
- R. Kuriki, H. Matsunaga, T. Nakashima, K. Wada, A. Yamakata, O. Ishitani, K. Maeda, *J. Am. Chem. Soc.* 138 (2016) 5159–5170.
- P.N. Paulino, V.M.M. Salim, N.S. Resende, *Appl. Catal. B-Environ.* 185 (2016) 362–370.
- A.J. Anceno, R.M. Stuetz, *Appl. Catal. B-Environ.* 181 (2016) 661–671.
- J.W. Jurss, J.J. Concepcion, J.M. Butler, K.M. Omberg, L.M. Baraldo, D.G. Thompson, E.L. Lebeau, B. Hornstein, J.R. Schoonover, H. Jude, J.D. Thompson, D.M. Dattelbaum, R.C. Rocha, J.L. Templeton, T.J. Meyer, *Inorg. Chem.* 51 (2012) 1345–1358.
- C.C. Hou, T.T. Li, S. Cao, Y. Chen, W.F. Fu, *J. Mater. Chem. A* 3 (2015) 10386–10394.
- K. Matsumoto, T. Matsumoto, M. Kawano, H. Ohnuki, Y. Shichi, T. Nishide, T. Sato, *J. Am. Chem. Soc.* 118 (1996) 3597–3609.
- P. Lei, M. Hedlund, R. Lomoth, H. Rensmo, O. Johansson, L. Hammarstrom, *J. Am. Chem. Soc.* 130 (2008) 26–27.
- D.J. Boston, C.D. Xu, D.W. Armstrong, F.M. MacDonnell, *J. Am. Chem. Soc.* 135 (2013) 16252–16255.
- J. Liu, H. Shi, X. Huang, Q. Shen, G. Zhao, *Electrochim. Acta* 216 (2016) 228–238.
- J.H. Jeon, P.M. Mareeswaran, C.H. Choi, S.I. Woo, *RSC Adv.* 4 (2014) 3016–3019.
- E.B. Cole, P.S. Lakkaraju, D.M. Rampulla, A.J. Morris, E. Abelev, A.B. Bocarsly, *J. Am. Chem. Soc.* 132 (2010) 11539–11551.
- G. Sahara, R. Abe, M. Higashi, T. Morikubo, K. Maeda, Y. Ueda, O. Ishitani, *Chem. Commun.* 51 (2015) 10722–10725.
- K. Sekizawa, K. Maeda, K. Domen, K. Koike, O. Ishitani, *J. Am. Chem. Soc.* 135 (2013) 4596–4599.
- T.W. Woolerton, S. Sheard, E. Reisner, E. Pierce, S.W. Ragsdale, F.A. Armstrong, *J. Am. Chem. Soc.* 132 (2010) 2132–2133.
- E. Kato, H. Takeda, K. Koike, K. Ohkubo, O. Ishitani, *Chem. Sci.* 6 (2015) 3003–3012.
- A. Nakada, K. Koike, K. Maeda, O. Ishitani, *Chem. Green* 18 (2016) 139–143.
- Y. Kuramochi, K. Fukaya, M. Yoshida, H. Ishida, *Chem. Eur. J.* 21 (2015) 10049–10060.
- I.M. Dixon, E. Lebon, G. Loustau, P. Sutra, L. Vendier, A. Igau, A. Juris, *Dalton Trans.* (2008) 5627–5635.
- A. Sepheridari, S.G. Chen, A. Stublla, P.G. Potvin, S. Morin, *Electrochim. Acta* 87 (2013) 236–244.
- S.C. Roy, O.K. Varghese, M. Paulose, C.A. Grimes, *Acs Nano* 4 (2010) 1259–1278.
- X. Huang, Q. Shen, J. Liu, N. Yang, G. Zhao, *Energy Environ. Sci.* 9 (2016) 3161–3171.
- D. Wang, X.Y. Pan, G.T. Wang, Z.G. Yi, *RSC Adv.* 5 (2015) 22038–22043.
- C. Wang, C. Shao, X. Zhang, Y. Liu, *Inorg. Chem.* 48 (2009) 7261–7268.
- V.R. de Mendonça, O.F. Lopes, R.P. Fregonesi, T.R. Giraldi, C. Ribeiro, *Appl. Surf. Sci.* 298 (2014) 182–191.
- F. Beriti, F. Malossi, F. Marchetti, M. Pineschi, *Chem. Commun.* 51 (2015) 13694–13697.